Nuclear Instruments and Methods in Physics Research A303 (1991) 79–87
North-Holland

Structure investigations of thin carbon foils

G. Dollinger and P. Maier-Komor
Physik Department, Technische Universität München, W-8046 Garching, Germany

A. Mitwalsky
Siemens AG, Research Laboratories, Otto-Hahn-Ring 6, W-8000 München 83, Germany

Carbon foils produced by laser plasma ablation-deposition (lpa-foils), by the glow discharge process (gd-foils) and by evaporation-condensation (ec-foils) were investigated by high resolution transmission electron microscopy and electron diffraction. A quantitative analysis is presented for the degree of anisotropic orientation of the quasi-graphitic nanocrystals in the polycrystalline foils. In the new type lpa-foils the nanocrystals are nearly isotropically oriented, in contrast to the anisotropic alignment in the ec- and gd-foils. This random orientation is responsible for a longer lifetime of lpa-foils when irradiated with heavy ions.

1. Introduction

Investigations of swift heavy ion induced effects in carbon stripper foils led to a model of the damage mechanism [1]. The model predicts that carbon foils with a structure of randomly oriented nanocrystals should experience minimum dimensional change and thus should survive the irradiation much longer than foils with an anisotropic crystal alignment. Since the stripper foil lifetime is dependent on the structure of the carbon foil, long lasting and expensive accelerator tests are not necessary to determine whether or not a specific preparation method can be utilized for lifetime improvement of carbon foils under heavy ion bombardment. Crystallographic structure investigations indicated that foils produced by the laser plasma ablation-deposition process [2] have a nearly isotropic distribution of nanocrystals and should demonstrate excellent lifetimes. This hypothesis was subsequently confirmed by measurements at the Munich tandem accelerator [3,4].

In this paper structure studies on common types of carbon foils will be presented. The foils studied were produced by evaporation-condensation [5] (ec-foils), by glow discharge in ethene gas (gd-foils) [6,7] and by laser plasma ablation-deposition (lpa-foils). The differences in structure will be demonstrated more qualitatively by means of electron diffraction in section 2 and high resolution transmission electron microscopy (HRTEM) in section 3. A quantitative analysis of the electron diffraction patterns will be given in section 4, which allows even very similar carbon structures to be compared.

2. Electron diffraction

All investigated foils had a thickness of about 4 $\mu g/cm^2$, which is the standard thickness of stripper foils used in the terminal of the Munich tandem accelerator. These thin foils are very suitable for transmission electron diffraction studies with 80 keV electrons, because disturbing energy loss and multiple scattering are negligible. The diffraction studies were done with a Philips EM 400 electron microscope.

Diffraction patterns from various carbon foils are shown in fig. 1. These patterns are caused by diffraction of electrons at crystal-lattice planes of nanocrystals which comprise the polycrystalline foils. The average length, L_{hkl}, of the crystallites in their (hkl)-direction (with Miller indices h, k and l) can be obtained from the following equation [8]:

$$L_{hkl} = 2\tilde{k} d_{hkl} \frac{s_{hkl}}{\Delta s_{hkl}}, \tag{1}$$

with $\tilde{k}$ a constant depending on the form of the crystallites. For spherical crystallites $\tilde{k}$ is about 0.9. The variable d_{hkl} is the separation of the (hkl)-planes, and $\Delta s_{hkl}/s_{hkl}$ the relative width (FWHM) of the (hkl)-diffraction ring.

The untreated ec-, gd- and lpa-foils show broad diffraction patterns (fig. 1a–c [9]). The corresponding average length of the crystallites is about 1 nm. This low spatial extension of the crystallites led for carbon foils, prepared by thermal evaporation, to the interpretation that these foils are amorphous [10], though electron diffraction shows some anisotropic structure which contradicts an amorphous state.

0168-9002/91/$03.50

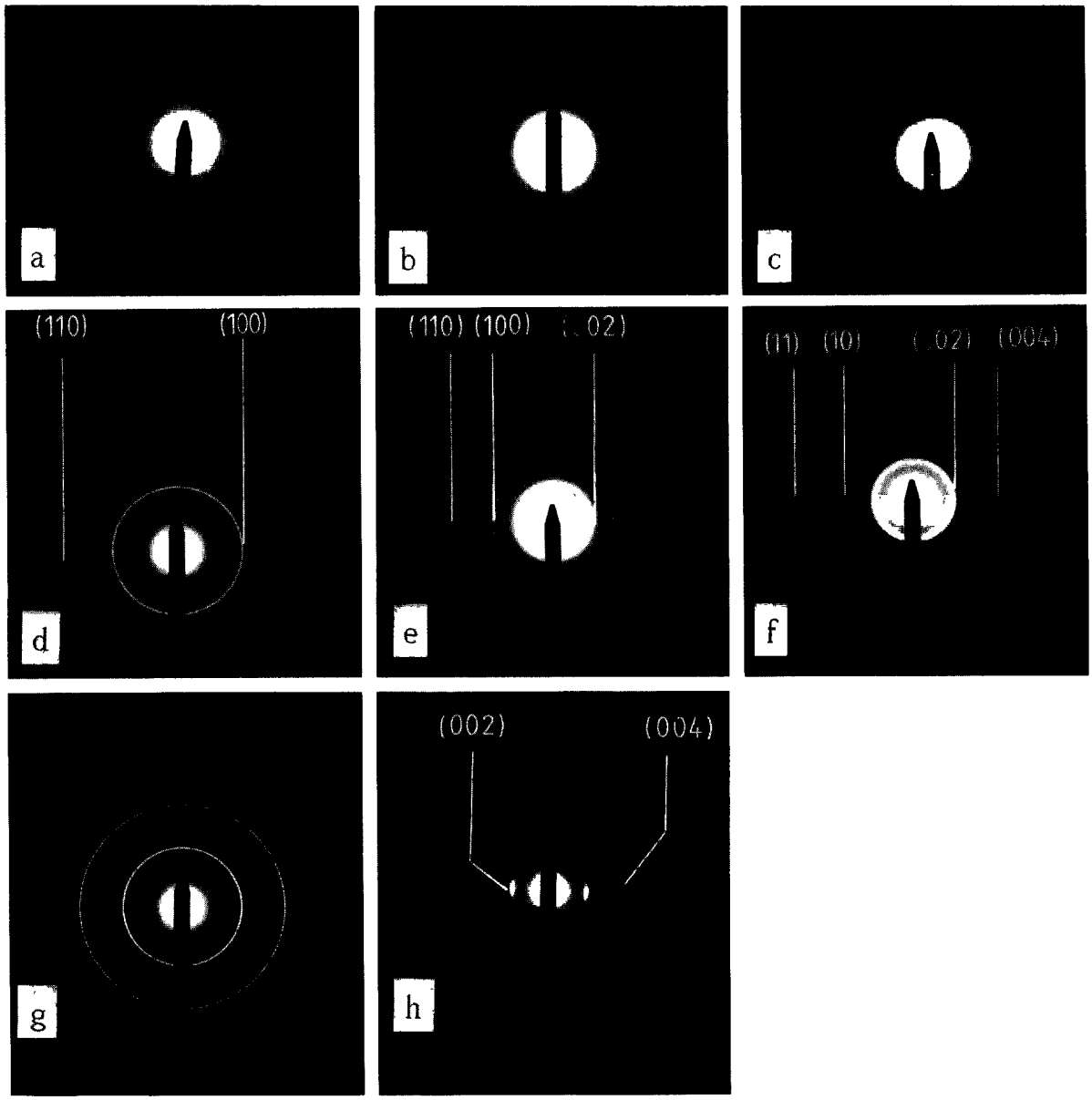

Fig. 1. Electron diffraction patterns of different carbon foils: (a) ec-foil, untreated; (b) gd-foil, untreated; (c) lpa-foil, untreated; (d) ec-foil, heat treated up to 2300 K; (e) gd-foil, heat treated up to 2300 K; (f) lpa-foil, heat treated up to 2300 K; (g) ec-foil, heat treated up to 4200 K; and (h) ec-foil, heat treated up to 4200 K. Portions of its surface are nearly parallel to the electron beam.

The anisotropy can be seen better in heat treated carbon foils. Heat treatment of the foils was accomplished using a Nd-YAG laser in high vacuum ($\approx 10^{-5}$ Pa) [5,9,11]. In fig. 1d–f diffraction rings of foils heated to 2200 K are shown. These rings are sharper than those of the untreated foils (fig. 1a–c) and correspond to about 5 nm large crystallites, which have been exogeneous due to the high temperature [9]. The diameters of the most intense rings are the same as for the (002)-, (100)- and (110)-rings of a pure graphite crystal. The graphite structure is shown in fig. 2 for illustration.

Generally heat treatment develops (002)-rings in diffraction patterns of gd- and lpa-foils (fig. 1e,f) but not in those of the anisotropic ec-foils. The diffraction angles are small ($\Theta_{002} \approx 6.2$ mrad) for 80 keV electrons. Therefore the crystal planes producing these observed diffractions must be nearly parallel to the electron beam [9]. Since normally the electron beam is perpendicular

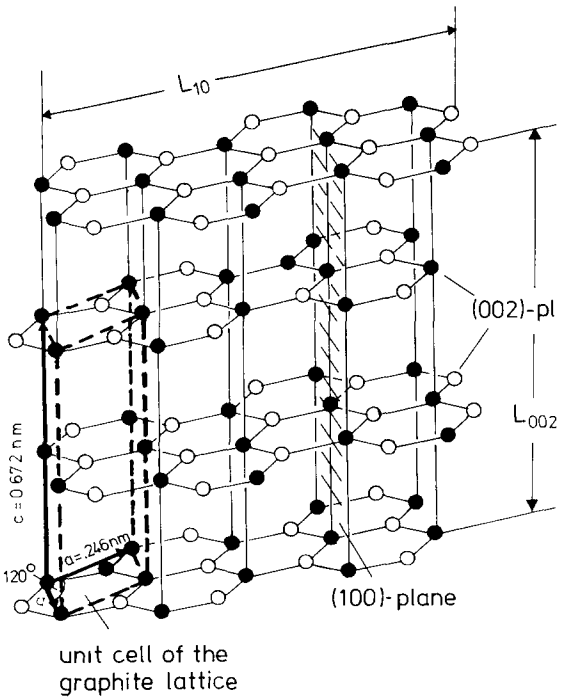

Fig 2. Schematic diagram of a graphite crystal.

to the foil surface, the lack of (002)-ring in ec-foils indicates the vast majority of their (002)-planes lie more parallel to the foil surface. Since all foils were heat treated the same way, and only the ec-foils did not develop (002)-rings, the anisotropy of crystallite orientation must have existed also prior to heat treatment.

The degree of anisotropy was measured by electron diffraction for an ec-foil, which had been heat treated up to 4200 K. The heat treatment was done as described in ref. [9], except that this time a Spectra Physics DCR-11 laser with its short (< 10 ns) light pulses was used [11]. The diffraction pattern for this ec-foil (fig. 1g) is sharper than for those heated to lower temperatures, but no other change is apparent. Eq. (1) indicates its crystallites have grown to about 10 nm.

The anisotropy of the ec-foils can be estimated from the diffraction pattern of fig. 1h, for which a foil was folded so that the beam was no longer perpendicular to the foil surface, but instead nearly parallel. This resulted in a partial development of the (002)-ring. The azimuthal extent of the (002)-ring corresponds to the distribution of angles of the (002)-planes to the foil surface and a small bending of the fold itself. Therefore a (002)-texture, which means a film growth direction along the (002)-lattice plane, can be observed. Due to the small bending of the fold itself only an upper limit of the deviation of the texture can be given, which is $\pm 25°$ total angle and $\pm 7°$ FWHM.

Another feature of the diffraction data indicates that all the foils are notably different from normal polycrystalline graphite. Although the ($hk0$)- and ($00l$)-rings of the diffraction patterns are essentially identical to those of graphite, there are no (hkl)-rings with h and l or k and l simultaneously non-zero. This same effect can be observed in special cases of bulk graphite (e.g. carbon black) [12,13]. This type of graphite consists of parallel (002)-planes with the normal graphite separation. However, the planes are shifted and rotated randomly relative to one another such that there are no three-dimensional periodic crystals and therefore no diffraction patterns with mixed Miller indices can be formed. For $l = 0$ this results in diffraction patterns of two-dimensional lattices, which then are called (hk)-rings with a characteristic intensity distribution. The shape of the (hk)-rings is asymmetrical with a long tail to large diffraction angles (see section 4). Therefore in fig. 1f the rings are labeled in this way, while in fig. 1d,e the standard three-dimensional characterization was chosen for comparison.

3. High resolution transmission electron microscopy (HRTEM)

The advantage of HRTEM is that crystal structures can be depicted in real space. 400 keV electrons from a JEOL 4000 EX electron microscope were used to image lattice planes of different carbon foils. By means of phase contrast the resolution limit of the apparatus is about 0.14 nm. A HRTEM image of an ec-foil, heat treated to about 4200 K and thinned to 1 $\mu g/cm^2$ by using three laser pulses in high vacuum, is shown in fig. 3. Some regions with parallel stripes can be seen. The distance between two adjacent stripes is 0.21 nm, which is the same as the distance d_{10} of the (10)-stripes of two-dimensional graphite (see fig. 2). Every region with parallel stripes is an image of one nanocrystal whose areal size can be directly measured. The average length of the crystallites is about 10 nm, consistent with the value determined by electron diffraction. Areas appearing cross-hatched or checked are due to two nanocrystals superimposed with different orientations. If the stripes of many crystallites are simultaneously imaged or not perfectly oriented with respect to the electron beam, only a random black and white contrast can be seen.

The texture of the heat treated ec-foils can be observed if a HRTEM image is taken from a region with the foil surface parallel to the electron beam. In fig. 4 the (002)-planes of such an area can be seen. These (002)-planes ($d_{002} = 0.34$ nm) are nearly parallel to the foil surface, which is characterized by the black and white border in the image. A bow of the foil in particular demonstrates that the direction of (002)-planes is always aligned parallel to the surface. Only small

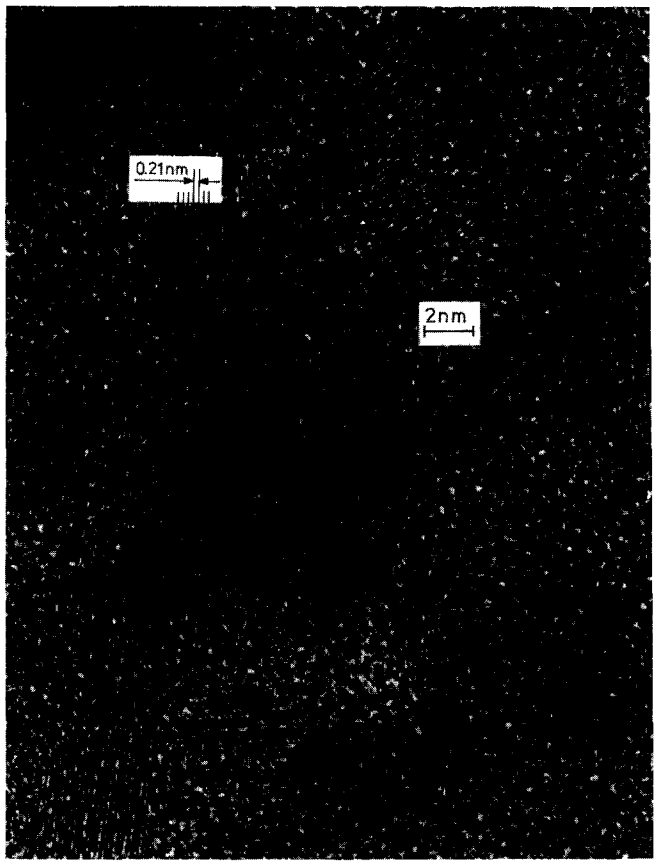

Fig. 3. High resolution transmission electron microscope (HRTEM) image of an ec-foil heat treated up to 4200 K. (10)-stripes (distance d_{10} = 0.21 nm) of some two-dimensional crystallites can be detected.

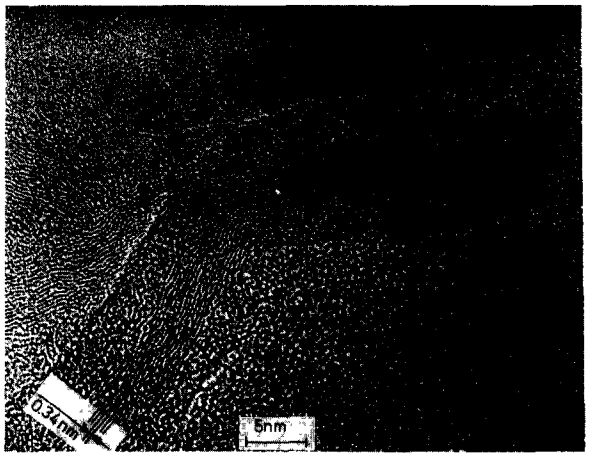

Fig. 4. HRTEM image of a heat treated ec-foil. The darker area is a part of the foil with its surface nearly parallel to the electron beam. Therefore those (002)-planes (distance d_{002} = 0.34 nm) which are nearly parallel to the foil surface become visible

regions of up to two (002)-layers with a perfect periodic structure can be observed. This demonstrates the two-dimensional character of the graphite crystallites.

Contrary to the case for ec-foils, the (002)-planes of lpa-foils can be imaged when the foil surface is perpendicular to the electron beam (fig. 5). The lpa-foil used for this picture was heat treated to 2200 K and had a thickness of 4 $\mu g/cm^2$. Twisted crystals can be detected sometimes with a nearly circular arrangement of the (002)-planes. The crystallites with their (002)-planes perpendicular to foil surface are randomly distributed resulting in a corresponding full ring in the diffraction pattern (fig. 1f).

4. Degree of orientation of the quasi-graphitic crystallites in different carbon foils

From the electron diffraction and HRTEM investigations discussed in section 2 and 3, it can be concluded that there are quasi-graphitic crystallites in lpa-foils

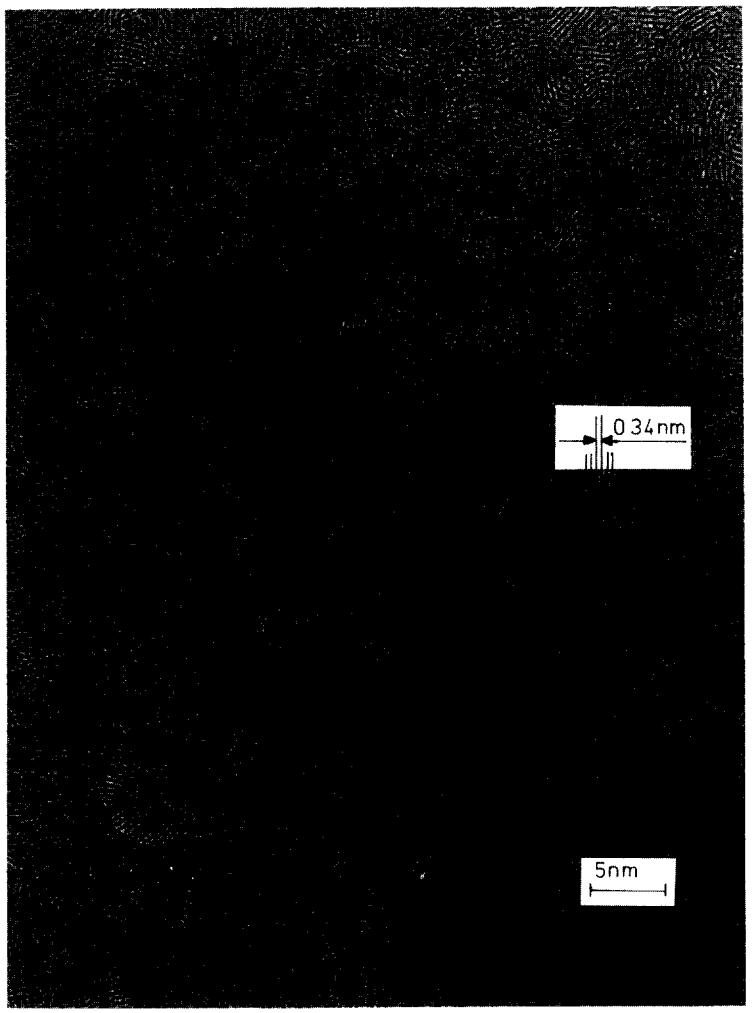

Fig. 5. HRTEM image of a heat treated (2200 K) lpa-foil. Crystallites with their (002)-planes perpendicular to the foil surface are visible. The planes are often bent and sometimes nearly circularly arranged.

with their (002)-planes nearly perpendicular to the foil surface. Their spatial and rotational distribution is of a random character. However, there is no further information on whether there is a complete isotropic distribution of the crystallites in relation to an axis parallel to the foil surface or whether there are differences between gd- and lpa-foils. Therefore a quantitative analysis of the electron diffraction patterns was conducted.

As a measure for a preferred orientation of the nanocrystals the ratio I_{002}/I_{10} is used. The integrated intensity I_{002} of an (002)-ring depends on the number of (002)-planes nearly perpendicular to the foil surface, while the integrated intensity I_{10} is proportional to the total number of the (10)-stripes with small corrections with respect to their orientation to the electron beam. The integrated intensities can be directly measured from the diffraction patterns with a densitometer.

4.1. Theoretical value of I_{002}/I_{10} for an isotropic distribution of crystallites

In the following the quantity I_{002}/I_{10} is calculated for an isotropic distribution of the crystallites in a carbon foil. It should be noted that electrons diffracted into the (002)-ring are scattered by three-dimensional structures of stacked (002)-planes. But electrons forming the (10)-ring are scattered at two-dimensional lattices of (10)-stripes in single (002)-planes. That is why the line shapes of their associated rings are different and the diffraction ring intensities for each case have to be calculated differently. A Debye–Scherrer ring of three-dimensional structures is caused by interference at planes with Miller indices h, k and l. Its integrated intensity I_{hkl} on a cylindrical film is given in ref. [14]. To get a form which can be compared to the

integrated intensities of two-dimensional rings, the formula of ref. [14] was changed into the following equation which is valid for a measurement of ring intensity in a plane perpendicular to the incident electron beam:

$$I_{hkl} = I_0 \frac{l_D}{r} \frac{N\lambda_e^3}{16\pi V_E} p_{hkl} |F_{hkl}|^2 \frac{\cos 2\Theta_{hkl}}{\sin^2\Theta_{hkl} \cos \Theta_{hkl}}. \quad (2)$$

I_0 is the incoming electron intensity, l_D is the length of the densitometer slit, r is the camera length, N denotes the number of unit cells in the illuminated foil area, V_E is the volume of a unit cell, Θ_{hkl} is the half scattering angle (Bragg angle) of the electrons diffracted at a (hkl)-plane and p_{hkl} is the geometric multiplicity of the (hkl)-planes.

$$|F_{hkl}| = \left| \sum_j f_j(\Theta_{hkl}) \exp\left(-2\pi i\left(hx_j + ky_j + lz_j\right)\right) \right|,$$

is the structure amplitude, where (x_j, y_j, z_j) are the coordinates of the jth basal atom in units of lattice vectors, and the sum is over all basal atoms of the unit cell. $f_j(\Theta_{hkl}) = 0.2393\ \lambda_e^2 (Z - f_{j,x}(\Theta_{hkl}))/\sin^2\Theta_{hkl}$ is the Born scattering length in nm for elastic scattering of electrons with wavelength λ_e (in nm) at the potential of an atom with atom number Z [15]. The scattering amplitude for X-rays $f_{j,x}(\Theta_{hkl})$ represents the screening of the nuclear potential by the atomic electrons. Numerical values for $f_j(\Theta_{hkl})$ were taken from ref. [15].

Eq. (2) results from a kinematical approximation of electron diffraction, which should be applicable for pure carbon crystallites smaller than 20 nm without marked uncertainties [16]. The calculated intensity corresponds to that measured with a densitometer.

Eq. (2) can also be obtained from the corresponding term for X-ray diffraction [17] by replacing the Thomson scattering length for X-rays and the structure amplitude by the Born scattering length and the structure amplitude for electrons. An expression for the integrated intensity I_{hk} of electrons diffracted from (hk)-stripes in a two-dimensional lattice onto a planar film can be similarly developed from the X-ray case originally derived by Warren [12]:

$$I_{hk} = I_0 \frac{l_D}{r} \frac{N_1 N_2 M \lambda_e^2}{4\pi A_a} p_{hk} |\tilde{F}_{hk}|^2 \frac{\cos 2\Theta_{hk}}{\sin \Theta_{hk}} \times \arcsin\left(\frac{\sqrt{1 - \sin^2\Theta_{hk}/\sin^2\Theta_{hk,\max}}}{\cos \Theta_{hk}} \right), \quad (3)$$

where N_1 and N_2 are the number of (hk)-stripes in the direction of the lattice vectors. Therefore $N_1 \times N_2$ is the number of elementary plane segments of a two-dimensional plane. M is the number of planes in the illuminated area, A_a is the area of an elementary plane segment and p_{hk} is the geometric multiplicity of a lattice stripe.

$$|\tilde{F}_{hk}| = \left| \sum_j f_j(\Theta_{hk}) \exp\left(-2\pi i\left(hx_j + ky_j\right)\right) \right|$$

is the structure amplitude of an elementary plane segment, and the sum extends over all basal atoms in such a segment. $2\Theta_{hk}$ is the minimum scattering angle of electrons scattered at a lattice of (hk)-stripes. The intensity of a two-dimensional (hk)-diffraction ring slowly decreases for $\Theta > \Theta_{hk}$. Therefore the integration of the intensity has to be performed to some limit, $\Theta_{hk,\max}$, leading to the dependency of I_{hk} on $\Theta_{hk,\max}$. $\Theta_{hk,\max}$ has to be big enough to get $\Theta_{hk,\max} - \Theta_{hk}$ larger than the half width of the (hk)-ring determined by the limited crystallite length (eq. (1)) [12]. The actual choice of $\Theta_{hk,\max}$ is discussed in the following section.

The desired quantity I_{002}/I_{10} can be derived by dividing eq. (2) by eq. (3). With the approximation $\sin\Theta \approx \Theta$ and $\cos\Theta \approx \cos 2\Theta \approx 1$ for small scattering angles 2Θ:

$$\frac{I_{002}}{I_{10}} = \frac{1}{4} \frac{N}{N_1 N_2 M} \frac{\lambda_e A_a \Theta_{10}}{V_E \Theta_{002}^2} \frac{p_{002} |F_{002}|^2}{p_{10} |\tilde{F}_{10}|^2} \times \frac{1}{\arcsin\sqrt{1 - (\Theta_{10}/\Theta_{10,\max})^2}}. \quad (4)$$

$N_1 N_2 M = 2N$, because there are two (002)-planes in each three-dimensional hexagonal unit cell (fig. 2). Bragg's rule leads to $\lambda_e = 2d_{002}\Theta_{002}$, where d_{002} is the distance between two neighbouring (002)-planes, which leads to $V_E = 2d_{002}A_a = \lambda_e A_a/\Theta_{002}$. The number p_{10} is 6, because a hexagonal lattice has 60°-symmetry about the (002)-axes. In the perpendicular direction there is only a mirror symmetry, which means $p_{002} = 2$. From these relations the following equation results:

$$\frac{I_{002}}{I_{10}} = \frac{d_{002}}{24 d_{10}} \frac{|F_{002}|^2}{|\tilde{F}_{10}|^2} \frac{1}{\arcsin\sqrt{1 - (\Theta_{10}/\Theta_{10,\max})^2}}. \quad (5)$$

Without reduction of generality the basal atoms in the three-dimensional quasi-graphitic lattice are located at the positions (0, 0, 0), $(\frac{1}{3}, \frac{2}{3}, 0)$, $(\alpha, \beta, \frac{1}{2})$ and $(\frac{2}{3} + \alpha, \frac{1}{3} + \beta, \frac{1}{2})$ with α and β arbitrary real numbers [12]. Therefore the structure amplitude is $|F_{002}| = 4f(\Theta_{002})$. In the two-dimensional unit plane there are only two atoms, one at the coordinates (0, 0) and one at $(\frac{1}{3}, \frac{2}{3})$, which means $|\tilde{F}_{10}| = f(\Theta_{10})$. For an exact calculation $f(\Theta_{002})$ and $f(\Theta_{10})$ should be weighted over the whole integration interval. As an approximation the scattering lengths $f(\Theta_{002}) = 0.175$ nm and $f(\Theta_{10}) = 0.123$ nm were used. Using in addition the known distances of graphite

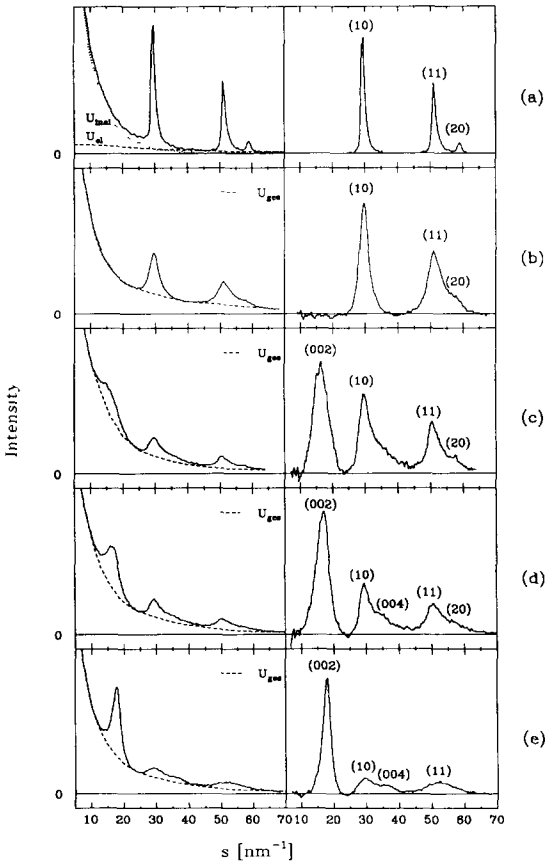

Fig. 6. Intensity distribution of the electron diffraction patterns measured with a densitometer. In the right column of the figure, the distribution after background subtraction is shown. (a) ec-foil, heat treated up to 4200 K; (b) ec-foil, heat treated up to 2200 K; (c) gd-foil, heat treated up to 2200 K; (d) lpa-foil, heat treated up to 2200 K; and (e) lpa-foil, irradiated with about 10^{15} $^{127}I^-$-ions/mm^2 (ion energy 10 MeV).

planes ($d_{002} = 0.336$ nm and $d_{10} = 0.213$ nm [18]) the intensity ratio can be written:

$$\frac{I_{002}}{I_{10}} = 2.13 \frac{1}{\arcsin\sqrt{1 - (\Theta_{10}/\Theta_{10,\max})^2}} . \qquad (6)$$

The chosen $s_{10,\max} = 45$ nm^{-1} (section 4.2), where $s = 4\pi \sin\Theta/\lambda_e$, results in $I_{002}/I_{10} = 2.5$ for an isotropic distribution of the nanocrystals.

4.2. Experimental determination of I_{002}/I_{10}

The ratio I_{002}/I_{10} was experimentally determined for different carbon foil structures. A PDS 1010A microdensitometer was used to measure intensity profiles along a diameter of diffraction rings directly from the film negatives. These profiles are shown in the left column of fig. 6 and are plotted as a function of $s = 4\pi \sin\Theta/\lambda_e$. The right column of fig. 6 shows the intensity profiles after background subtraction. Fig. 6a is from diffraction rings of an ec-foil, which had been heat treated up to 4200 K. Foils measured for fig. 6b (ec-foil), fig. 6c (gd-foil) and fig. 6d (lpa-foil) were heat treated up to 2200 K. Fig. 6e shows the profile of a lpa-foil which had been irradiated with about 10^{15} $^{127}I^-$-ions/mm^2 at 10 MeV. The two-dimensional characteristic of the crystal structure can be seen at the asymmetric densitometer plots of the (10)- and (20)-rings in figs. 6c–e with the long tails to large s-values. Due to the texture these tails cannot be seen in figs. 6a,b.

Determination of background intensity was done in the standard way, using two additive parts U_{el} and U_{inel} representing the elastical and inelastic scattering of electrons, respectively. U_{el} is generated by electron scattering at non-crystalline material or lattice defects and is proportional to $|f(\Theta)|^2$, i.e. $U_{el} = g|f(\Theta)|^2$ with a factor g which was experimentally determined. U_{inel} represents electron–electron scattering, which leads to larger energy losses. U_{inel} can only be empirically determined [19]. This was carried out, using the diffraction patterns of fig. 6a. Their peak widths are small enough to fit the background at the peaks with a straight line. U_{el} strongly outweighs U_{inel} at large s-values. Thus the factor g was fitted to get the total background U_{gem} for large s-values with U_{el}. Then U_{inel} was calculated as the difference $U_{gem} - U_{el}$.

U_{el} and U_{inel} are both plotted in fig. 6a (left column). The backgrounds of the other intensity profiles were determined by fitting the sum $aU_{inel} + bU_{el} + c$ with free parameters a, b and c to the background. The integration was performed numerically after background subtraction. The higher integration limit for I_{10} was chosen as $s_{10,\max} = 45$ nm^{-1} ($s_{10} = 29.5$ nm^{-1}), which is slightly before the (11)-intensity contributes markedly. In this integration interval the (004)-ring is also included ($s_{004} = 37.5$ nm^{-1}) and can be seen at the falling flanks of the (10)-peaks in fig. 6c–e. The integrated intensity I_{004} of the (004)-ring can be calculated from I_{002}, because from eq. (2) it is found that $I_{002}/I_{004} = 14.5$. Therefore I_{10} was calculated by integration of the intensity between $s = 25$ nm^{-1} and $s = 45$ nm^{-1} after subtraction of the background and the contribution of I_{004}.

4.3. Results

Table 1 compares the experimentally determined values of I_{002}/I_{10} to those theoretically calculated using eq. (6), which assumes an isotropic distribution of crystallites. The uncertainty of the experimentally determined values is about 30% and is attributed to uncertainties inherent in the background determinations, particularly at small s-values. The measured intensity ratio I_{002}/I_{10} for lpa-foils is close to the theoretically predicted one for an isotropic distribution of the quasi-

Table 1
Integrated intensity ratios I_{002}/I_{10} and crystallite lengths determined from half widths of the electron diffraction rings for different carbon foils

		I_{002}/I_{10}	Crystallite lengths [nm]	
			L_{002}	L_{10}
Theoretical values	No (002)-planes perpendicular to the foil surface	0		
	Isotropic arrangement of nanocrystallites	2.5		
ec-Foil (4200 K)		0	–	10
ec-Foil (2200 K)		0	–	4.8
gd-Foil (2200 K)		1.3	2.3	5.0
lpa-Foil (2200 K)		2.2	2.5	5.0
lpa-Foil irradiated with heavy ions		3.5	4.3	3.7

graphitic crystallites, while for the gd-foil I_{002}/I_{10} is only about half the theoretically predicted value and much smaller than for a lpa-foil. This suggests that the crystallites in lpa-foils are nearly isotropically distributed, while the gd-foils have a disproportionate share of their (002)-planes parallel to the foil surface and the ec-foils have nearly all their (002)-planes lying parallel to the foil surface.

4.4. Heavy ion irradiated lpa-foils

The described investigations were also done with a lpa-foil which had been irradiated with 0.72 pmC $^{127}I^-$-ions (10 MeV) in a central area of about 1 mm^2, which means 4.5×10^{15} ions/mm^2. The ion current was about 300 nA/mm^2. Therefore a temperature of about 1300 K was achieved during irradiation [1]. But the central part of the irradiated area dropped out either during irradiation or subsequent venting and could not be saved. Therefore the zone adjacent to the hole, which should have been irradiated with nearly the same dose, was investigated. There the dose was high enough to reduce the thickness from originally 4.1 μg/cm^2 to 3 μg/cm^2, which could be measured by electron transmission in an electron microscope [20].

The data of table 1 show that the high temperature caused by the ion irradiation resulted in an average length of the (10)-planes of about 3.7 nm. In the (002)-direction the crystallites of the irradiated lpa-foils are higher ($L_{002} = 4.3$ nm) than in (10)-direction in contrast to the non-irradiated lpa-foils. This is a consequence of the new (002)-planes, which build up between the original planes during the irradiation and which result in an increase of L_{002} as was predicted in ref. [1].

It is surprising that the number of crystallites with their (002)-planes perpendicular to the lpa-foil surface increases, because I_{002}/I_{10} is larger than in non-irradiated lpa-foils. I_{002}/I_{10} is even larger than calculated for an isotropic distribution of the crystallites. This proves a preferred direction of the (002)-planes perpendicular to the foil surface in an heavy ion irradiated lpa-foil, just the opposite direction of the anisotropy in ec- or gd-foils. Generally, a heavy ion beam penetrating a carbon foil perpendicularly to the foil surface influences the growth of graphitic crystallites with their (002)-planes perpendicular to the foil surface. Already in ec-foils the described anisotropy (section 2) with the (002)-planes nearly parallel to the foil surface is partly disturbed by heavy ion irradiation [1].

5. Conclusion

It was shown that electron microscopy and electron diffraction are valuable tools when used in the investigation of thin carbon foils. This is particularly evident in structure studies of heat treated foils, where dimensions, structure and spatial distribution characteristics of their nanocrystals can be quantitatively determined. This characterization allows carbon foils produced by different means to be readily compared. Specifically, as regards stripper foils performance, lpa-foils have the best qualifications, because foils with a nearly isotropic orientation of the quasi-graphitic nanocrystals should show the longest lifetimes [1]. This has been verified by means of irradiation tests with ec-, gd- and lpa-foils [3,11].

Therefore these structure studies perform a quick and reliable test of whether a new carbon foil preparation technique can produce carbon foils with good stripper qualities.

Acknowledgement

This work was supported by the German Federal Ministry for Research and Technology (BMFT) under contract 06 TM 108.

References

[1] G. Dollinger and P. Maier-Komor, Nucl. Instr. and Meth. A282 (1989) 223.
[2] G. Dollinger and P. Maier-Komor, these Proceedings (15th World Conf. of the INTDS, Santa Fe, NM, 1990) Nucl. Instr. and Meth. A303 (1990) 50.
[3] G. Dollinger and P. Maier-Komor, Nucl. Instr. and Meth. B53 (1991) 352.
[4] G. Dollinger and P. Maier-Komor, Proc. SNEAP 1989, Oak Ridge (World Scientific, New Jersey, 1990) p. 138.
[5] P Maier-Komor, E. Ranzinger and H. Münzer, Nucl. Instr. and Meth. 200 (1982) 5.
[6] B. Huck, Ph.D. thesis, Heidelberg, FRG, 1981.
[7] B. Huck, E. Jaeschke, W. Kratschmer, R. Repnow and H. Wirth, Nucl. Instr. and Meth. 184 (1981) 215.
[8] A. Glauert, Practical Methods in Electron Microscopy, vol. 1 (North-Holland, London, 1972) p. 311.
[9] G. Dollinger and P. Maier-Komor, Nucl. Instr. and Meth. A257 (1987) 64.
[10] J. Kakinoki, K. Katada, T. Hanawa and T. Ino, Acta Crystallogr. 13 (1960) 171.
[11] G. Dollinger, Ph.D. thesis. TU München, FRG, 1990.
[12] B.E. Warren, Phys. Rev. 59 (1941) 693.
[13] J. Biscoe, B.E. Warren, J. Appl. Phys. 13 (1942) 364.
[14] M. v. Laue, Materiewellen und ihre Interferenzen (Akademische Verlagsgesellschaft, Leipzig, 1944) p. 149.
[15] International Tables for X-ray Crystallography vol. 3, ed. K. Londsdale (Kynoch Press, Birmingham, 1962) p. 217.
[16] M. Horstmann and G. Meyer, Acta Crystallogr. 15 (1962) 271.
[17] International Tables for X-ray Crystallography vol. 2, ed. K. Londsdale (Kynoch Press, Birmingham, 1959) p. 314.
[18] R Wyckoff, Crystal Structures, vol. 1 (Wiley, New York, 1965) p. 26
[19] R. Leonhardt, H Richter and W. Rossteutscher, Z. Phys. 165 (1961) 121
[20] G. Dollinger and P. Maier-Komor, Nucl. Instr. and Meth. A282 (1989) 153.